NASA Technical Memorandum 84492

Influence of Surface Static-Pressure Orifices on Boundary-Layer Transition

Dan M. Somers, John P. Stack,
and William D. Harvey
Langley Research Center
Hampton, Virginia

National Aeronautics
and Space Administration

**Scientific and Technical
Information Office**

1982

INTRODUCTION

One of the more important measurements to be made in wind-tunnel or flight testing is the distribution of local static pressure over the test surface. This distribution is usually determined by means of orifices connected via tubing to pressure transducers. The diameter of the orifice and the diameter and the length of the tubing can, however, affect the local flow and influence the measured static pressure. (See refs. 1 to 3.) In addition, the fluid in the orifice can be set in motion by the external flow. (See ref. 3.) As an example, an orifice could generate a disturbance within a laminar boundary layer which could cause premature transition. This disturbance could be caused by a Helmholtz resonance within the connecting tubing. (See ref. 3.) Additional effects on the boundary layer can result if the orifice has burrs, rounded edges, or other imperfections or if a number of orifices are aligned with the flow.

A fundamental study of the interaction of a turbulent boundary layer and surface static-pressure orifices on a flat plate was reported in reference 3. The results from that study indicate that the boundary layer downstream of the orifice was significantly altered by the orifice.

The present investigation is primarily concerned with the interaction of a laminar boundary layer and surface static-pressure orifices. The investigation was conducted on an airfoil designed to achieve extensive natural laminar flow, the NASA NLF(1)-0215F. (See ref. 4.) The effects of both favorable and adverse pressure gradients were studied. No three-dimensional configurations were tested.

The investigation was conducted in the Langley Low-Turbulence Pressure Tunnel (LTPT) (ref. 5) at Reynolds numbers based on airfoil chord from approximately 0.5×10^6 to 6.0×10^6 with Mach number varying accordingly from about 0.03 to 0.42.

SYMBOLS

Values are given in both SI and U.S. Customary Units. Measurements and calculations were made in U.S. Customary Units.

C_f boundary-layer skin-friction coefficient

C_p pressure coefficient

c airfoil chord, cm (in.)

d diameter of orifice, mm (in.)

l length of tubing, mm (in.)

M free-stream Mach number

R Reynolds number based on free-stream conditions and airfoil chord

R_d Reynolds number based on local conditions and orifice diameter

R_{δ^*} Reynolds number based on local conditions and boundary-layer displacement thickness

R_θ Reynolds number based on local conditions and boundary-layer momentum thickness

x airfoil abscissa, cm (in.)

x_T transition location, cm (in.)

y model spanwise station, cm (in.)

α angle of attack relative to chord line, deg

δ^* boundary-layer displacement thickness, mm (in.)

EXPERIMENTAL PROCEDURE

Wind Tunnel

The Langley Low-Turbulence Pressure Tunnel (LTPT) (ref. 5) is a continuous-flow, variable-pressure wind tunnel with controls which permit the independent variation of stagnation pressure and Mach number. The test section is 91.44 cm (36.00 in.) wide by 228.6 cm (90.00 in.) high. Hydraulically actuated circular plates provide positioning and attachment for the two-dimensional model. The plates, 101.6 cm (40.00 in.) in diameter, are flush with the tunnel sidewalls and rotate with the model. The model ends were mounted to rectangular model-attachment plates as shown in figure 1.

Model

The forward portion of the wind-tunnel model of the NASA NLF(1)-0215F airfoil consisted of an aluminum spar surrounded by black plastic filler with two thin layers of fiberglass forming the aerodynamic surface. The 25-percent-chord, simple flap was constructed of aluminum and attached to the forward portion of the model by aluminum brackets. The flap was not deflected during these tests. The model had a chord of 60.960 cm (24.000 in.) and a span of 91.44 cm (36.00 in.). Upper- and lower-surface chordwise orifices were located 7.62 cm (3.00 in.) to one side of the midspan at the chord stations listed in table I(a). Spanwise orifices were located in the upper surface at the chord and span stations listed in table I(b). All these orifices were 1.0 mm (0.040 in.) in diameter with the axes perpendicular to the surface. A sketch of a typical orifice and a close-up photograph are shown in figure 2. The connecting tubes were approximately 2.4 m (8.0 ft) in length, closed at the ends, and contained no sharp bends. (The radius of the tube was much larger than the inside diameter of the tube.) In addition, blind orifices having diameters of 0.25 mm (0.010 in.), 0.51 mm (0.020 in.), and 1.0 mm (0.040 in.) were drilled to various depths at the chord and span stations listed in table II. These orifices, of course, had no connecting tubes. The locations of all the upper-surface orifices (chordwise, spanwise, and blind) are shown in figure 3. The model surface was sanded with No. 600 dry silicon carbide paper to insure an aerodynamically smooth finish.

Tests and Methods

The model was tested at Reynolds numbers based on airfoil chord from approximately 0.5×10^6 to 6.0×10^6 with Mach number varying accordingly from about 0.03 to 0.42.

For all the runs in the test, the model upper surface was coated with oil to determine the location as well as the nature of the boundary-layer transition from laminar to turbulent flow. (See ref. 6.) After the oil-flow pattern had stabilized, photographs were taken. The run was then terminated and the pattern was inspected and recorded with sketches and measurements to aid in the interpretation of the photographs. It should be noted that a marked contrast between the forward portion of the model and the flap exists in all the oil-flow photographs because of the different materials used for the two surfaces - black plastic and bare aluminum, respectively. (See fig. 1.)

No static-pressure measurements were made. The pressure distributions for comparable conditions had been obtained previously. (See ref. 4.)

DISCUSSION OF RESULTS

Oil-Flow Patterns

The pressure distribution for the NLF(1)-0215F airfoil at an angle of attack of 0.0° for a Reynolds number of 3.0×10^6 and a Mach number of 0.10 is shown in figure 4. At this angle of attack, a favorable pressure gradient exists along the upper surface to about 0.40c. The oil-flow patterns on the upper surface at this angle of attack for various Reynolds numbers are shown in figure 5. The turbulent wedges in figures 5(d) to 5(f) were caused by contaminants in the oil. No orifice-induced disturbances are apparent for the forward 0.40c of the upper surface at any of the Reynolds numbers tested at this angle of attack.

The pressure distribution at an angle of attack of 5.0° for a Reynolds number of 3.0×10^6 and a Mach number of 0.10 is shown in figure 6. At this angle of attack, an adverse pressure gradient exists along the upper surface from about 0.05c to the trailing edge. The oil-flow patterns on the upper surface at this angle of attack for various Reynolds numbers are shown in figure 7. For $R = 0.5 \times 10^6$ and 1.0×10^6 (figs. 7(a) and 7(b), respectively), no orifice-induced disturbances are apparent. For $R = 1.5 \times 10^6$ (fig. 7(c)), premature transition occurs downstream of the largest forward orifices (d = 1.0 mm (0.040 in.)). For this Reynolds number, the orifices do not induce the classic turbulent wedges typical of three-dimensional disturbances. Instead, they induce disturbances which are carried downstream resulting in the "scallop-shaped," turbulent regions shown in figure 7(c). For $R = 2.0 \times 10^6$ (fig. 7(d)), the scallops occur downstream of the larger forward orifices (d = 0.51 mm (0.020 in.) and 1.0 mm (0.040 in.)) and farther forward than for $R = 1.5 \times 10^6$. The single wedge shown in figure 7(d) is the result of a contaminant in the oil. For $R = 3.0 \times 10^6$ (fig. 7(e)), the scallops occur downstream of orifices of all three diameters and have moved farther forward. A turbulent wedge that originates at the chordwise orifice row has also formed. This wedge has a spreading angle comparable to that of the classic turbulent wedge. (For example, see ref. 7.) The other two wedges shown in figure 7(e) are the result of contaminants. The pattern shown in figure 7(e) continues to move forward with increasing Reynolds number. (See figs. 7(f) and 7(g).)

Experimental Results

The effect of tube length-to-diameter ratio for single orifices on transition location on the upper surface at $\alpha = 5.0°$ (adverse pressure gradient) is shown in figure 8. The transition location is influenced by ℓ/d, although the trend for a given diameter is not consistent over the Reynolds number range of this investigation. The transition locations corresponding to the orifices with an ℓ/d of 2400 are close to those corresponding to the orifices with lower ℓ/d ratios. However the trend between the lower ℓ/d ratios and an ℓ/d of 2400 is not known and, therefore, no curve has been faired for that portion of figure 8. It is apparent, however, that the orifices with smaller diameters have less influence.

Additional correlations were attempted with the following parameters: d/δ^*, R_{δ^*}, R_θ, R_d, $R_d\sqrt{C_f/2}$, and $R(d/c)\sqrt{C_f/2}$. None was successful. This was not too surprising in that none of these "accepted" parameters contained the length of the tube.

CONCLUDING REMARKS

An investigation of the interaction of a laminar boundary layer and surface static-pressure orifices was conducted on a natural-laminar-flow airfoil, the NASA NLF(1)-0215F, in the Langley Low-Turbulence Pressure Tunnel. The effects of both favorable and adverse pressure gradients were studied at Reynolds numbers based on airfoil chord from approximately 0.5×10^6 to 6.0×10^6 with Mach number varying accordingly from about 0.03 to 0.42.

It was found that the smaller the diameter of the orifice, the less likely it will cause premature transition. Other considerations will, of course, limit the reduction in orifice diameter. Locating the orifices in a chordwise row aligned with the flow appears to have an additive, adverse effect on transition. Tube length-to-orifice diameter ratio does not seem to have a consistent influence on transition.

Langley Research Center
National Aeronautics and Space Administration
Hampton, VA 23665
June 9, 1982

REFERENCES

1. Shaw, R.: The Influence of Hole Dimensions on Static Pressure Measurements. J. Fluid Mech., vol. 7, pt. 4, Apr. 1960, pp. 550-564.

2. Franklin, R. E.; and Wallace, James M.: Absolute Measurements of Static-Hole Error Using Flush Transducers. J. Fluid Mech., vol. 42, pt. 1, June 4, 1970, pp. 33-48.

3. Moulden, T. H.; Wu, J. M.; Collins, F. G.; Ramm, H. J.; Kuwand, H.; Wu, C. I.; and Ray, R.: Experimental Study of Static Pressure Orifice Interference. AEDC-TR-77-57, U.S. Air Force, June 1977. (Available from DTIC as AD A046 403.)

4. Somers, Dan M.: Design and Experimental Results for a Flapped Natural-Laminar-Flow Airfoil for General Aviation Applications. NASA TP-1865, 1981.

5. Von Doenhoff, Albert E.; and Abbott, Frank T., Jr.: The Langley Two-Dimensional Low-Turbulence Pressure Tunnel. NACA TN 1283, 1947.

6. Loving, Donald L.; and Katzoff, S.: The Fluorescent-Oil Film Method and Other Techniques for Boundary-Layer Flow Visualization. NASA MEMO 3-17-59L, 1959.

7. Schubauer, G. B.; and Klebanoff, P. S.: Contributions on the Mechanics of Boundary-Layer Transition. NACA Rep. 1289, 1956. (Supersedes NACA TN 3489.)

TABLE I.- CHORDWISE AND SPANWISE ORIFICES

[c = 60.960 cm (24.000 in.), d = 1.0 mm (0.040 in.), ℓ/d = 2400]

(a) Chordwise

x/c	y/c
0.00034	0.12417
.00570	.12446
.01065	.12411
.01542	.12402
.02033	.12430
.02545	.12450
.03083	.12417
.04039	.12474
.05059	.12453
.06058	.12417
.07545	.12409
.10064	.12451
.15077	.12408
.20071	.12432
.25074	.12433
.30081	.12449
.35098	.12430
.40048	.12442
.45053	.12443
.50089	.12398
.55044	.12398
.60092	.12428
.65068	.12413
.70050	.12409
.74660	.12407
.80261	.12512
.85185	.12517
.90194	.12532
.95078	.12576
.97480	.12538

(b) Spanwise

x/c	y/c
0.05039	0.20714
.05134	.29105
.05196	.37410
.05265	.45734
.05333	.54113
.05419	.62328
.05434	.70698
.90229	.20805
.90182	.29160
.90224	.37444
.90225	.45785
.90204	.54144
.90205	.62478
.90224	.70866

TABLE II.- BLIND ORIFICES

[c = 60.960 cm (24.000 in.)]

x/c	y/c	d		l/d
		mm	in.	
0.07558	0.04079	1.0	0.040	25
.10043	.04087	1.0	.040	25
.15116	.04084	1.0	.040	26
.20096	.04127	1.0	.040	25
.25121	.04109	1.0	.040	25
.30085	.04110	1.0	.040	26
.35089	.04109	1.0	.040	26
.05030	-.07923	1.0	.040	21
.05034	-.15435	.51	.020	30
.05038	-.22934	.25	.010	34
.05028	-.30395	1.0	.040	13
.05031	-.37941	.51	.020	23
.05023	-.45423	.25	.010	15
.05001	-.52878	1.0	.040	6.2
.05022	-.60412	.51	.020	13
.05027	-.67907	.25	.010	26
.20096	-.04195	1.0	.040	25
.20066	-.11710	1.0	.040	25
.20088	-.19186	.25	.010	31
.20083	-.26699	.51	.020	30
.20069	-.34201	1.0	.040	12
.20071	-.41700	.25	.010	12
.20081	-.49204	.51	.020	25
.20077	-.56677	1.0	.040	6.8
.20071	-.64188	.51	.020	13

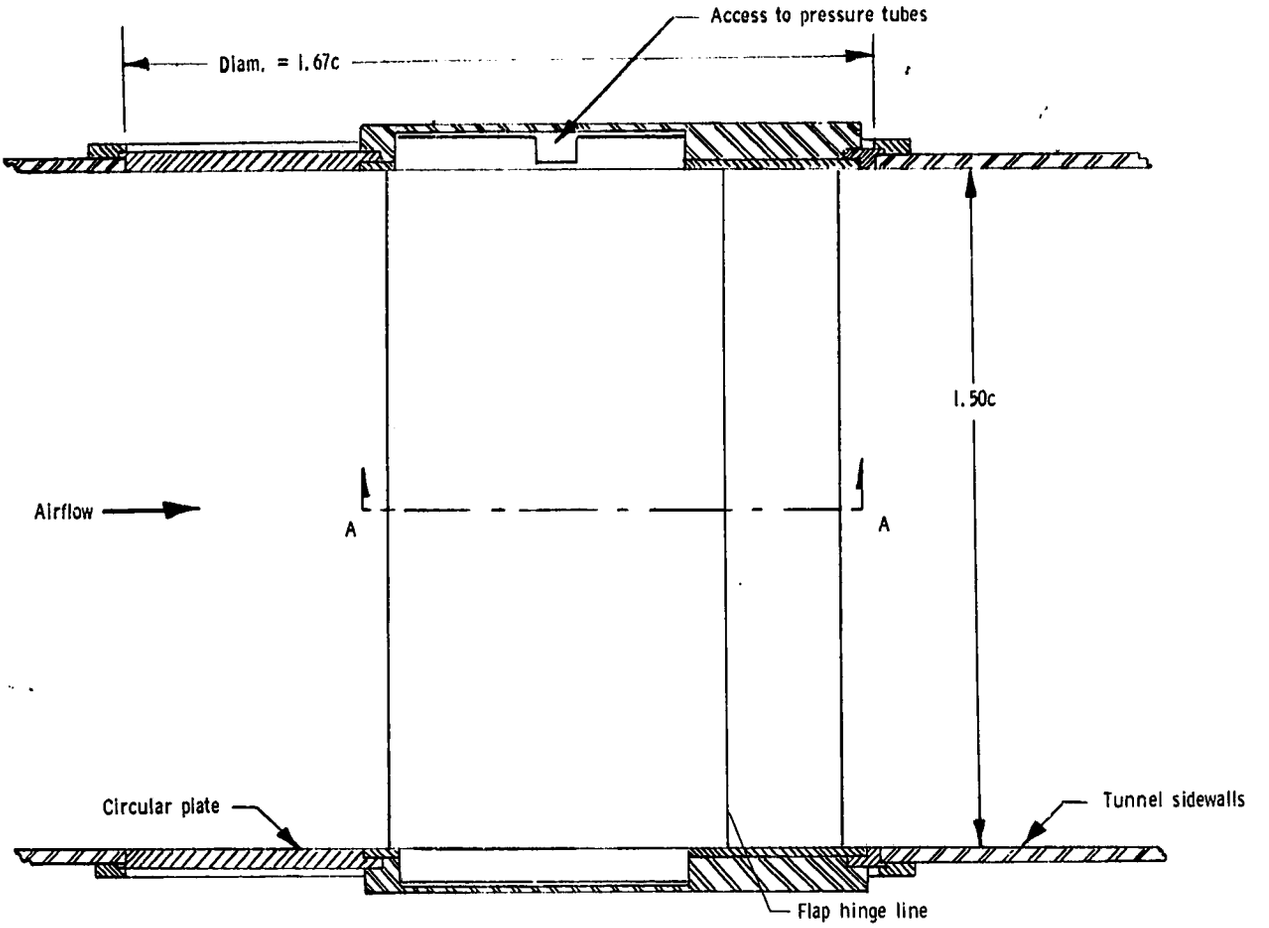

Top view

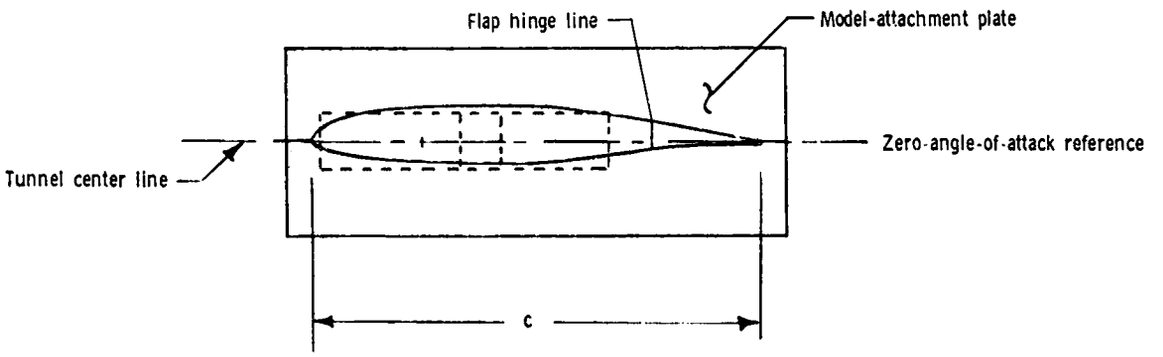

End view, section A-A

Figure 1.- Sketch of typical airfoil model mounted in the Langley Low-Turbulence Pressure Tunnel. All dimensions are in terms of model chord. c = 61.0 cm (24.0 in.).

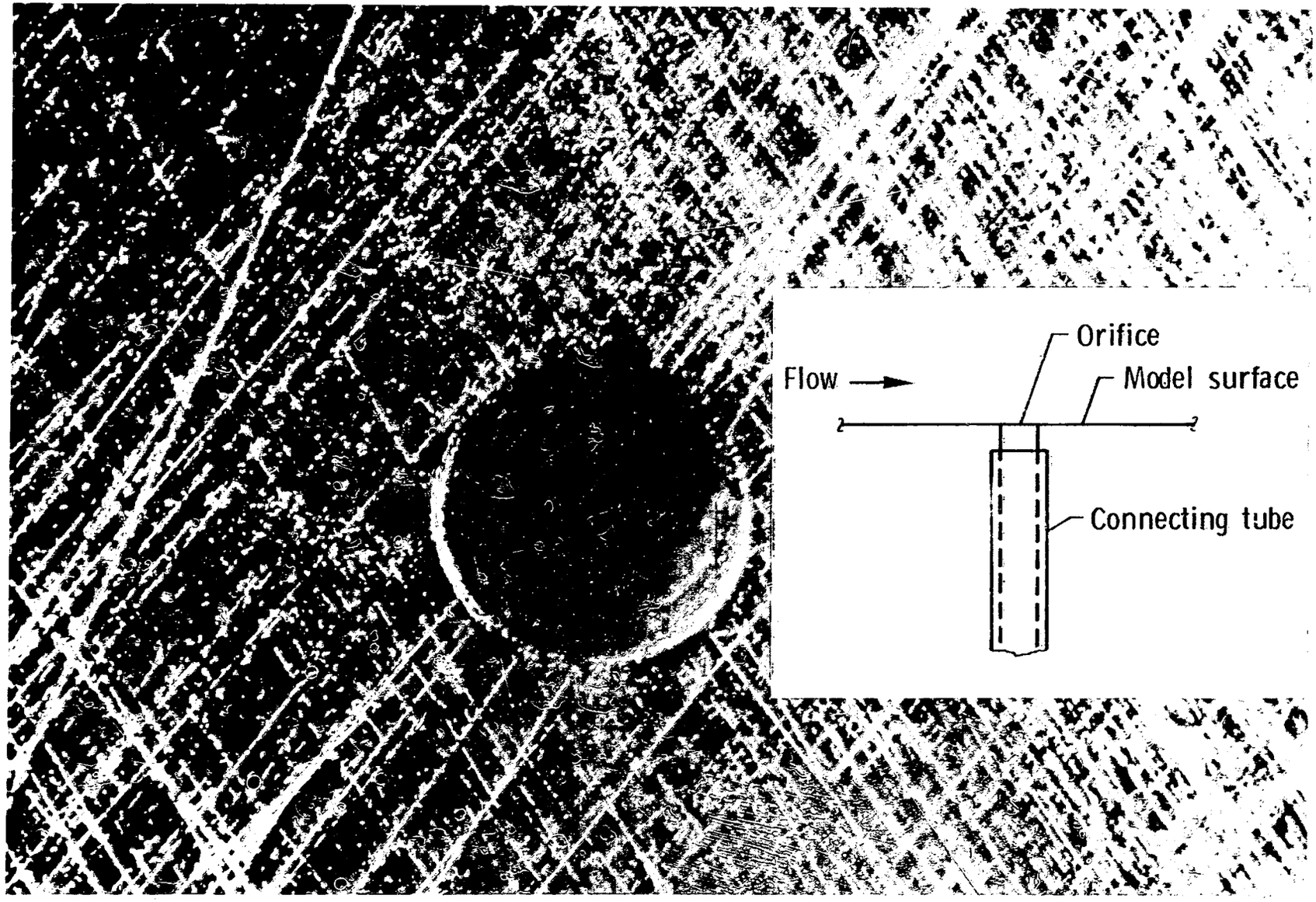

Figure 2.- Sketch and close-up photograph of typical orifice.

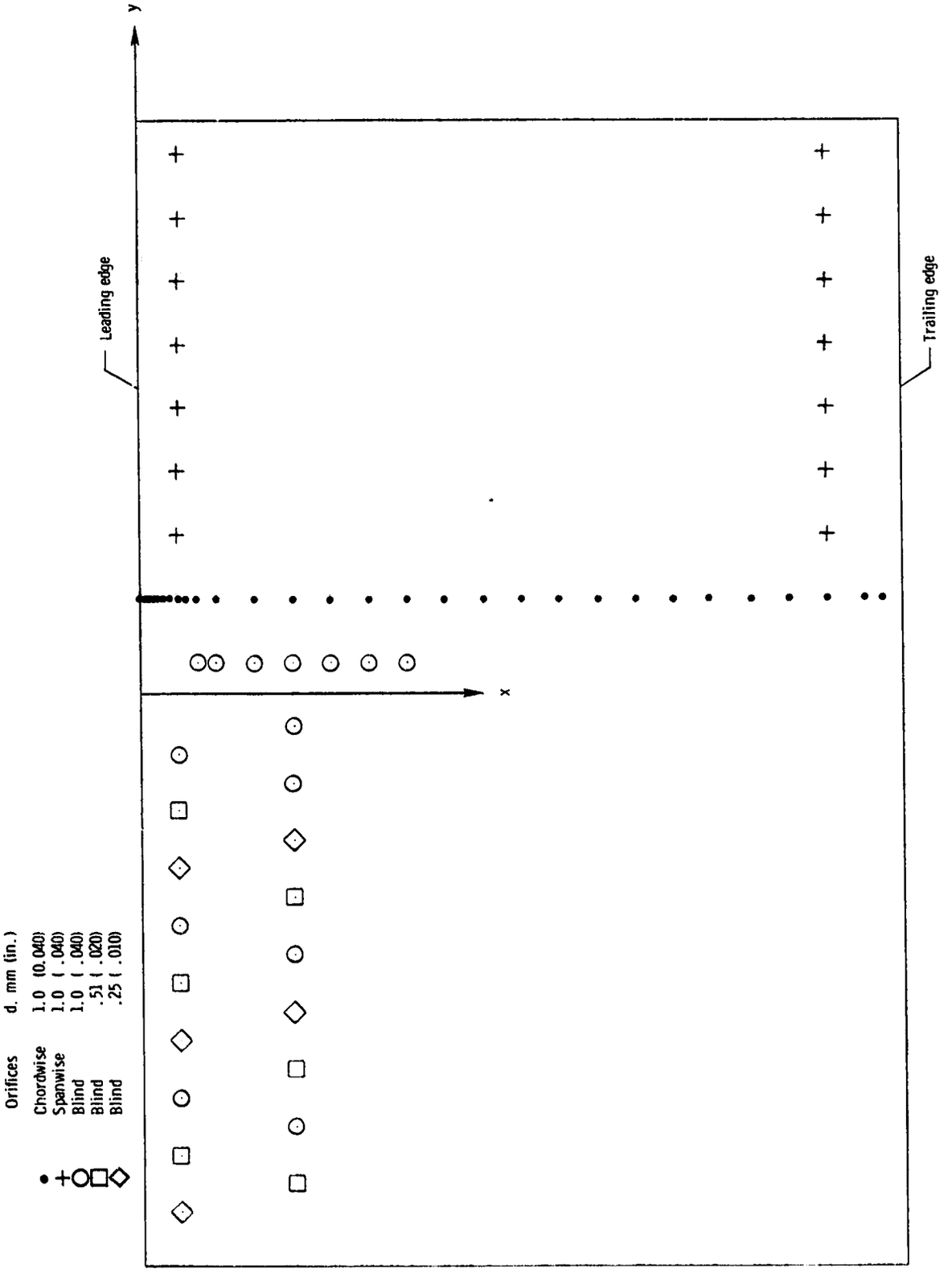

Figure 3.- Locations of orifices in upper surface of NFL(1)-0215F airfoil model.

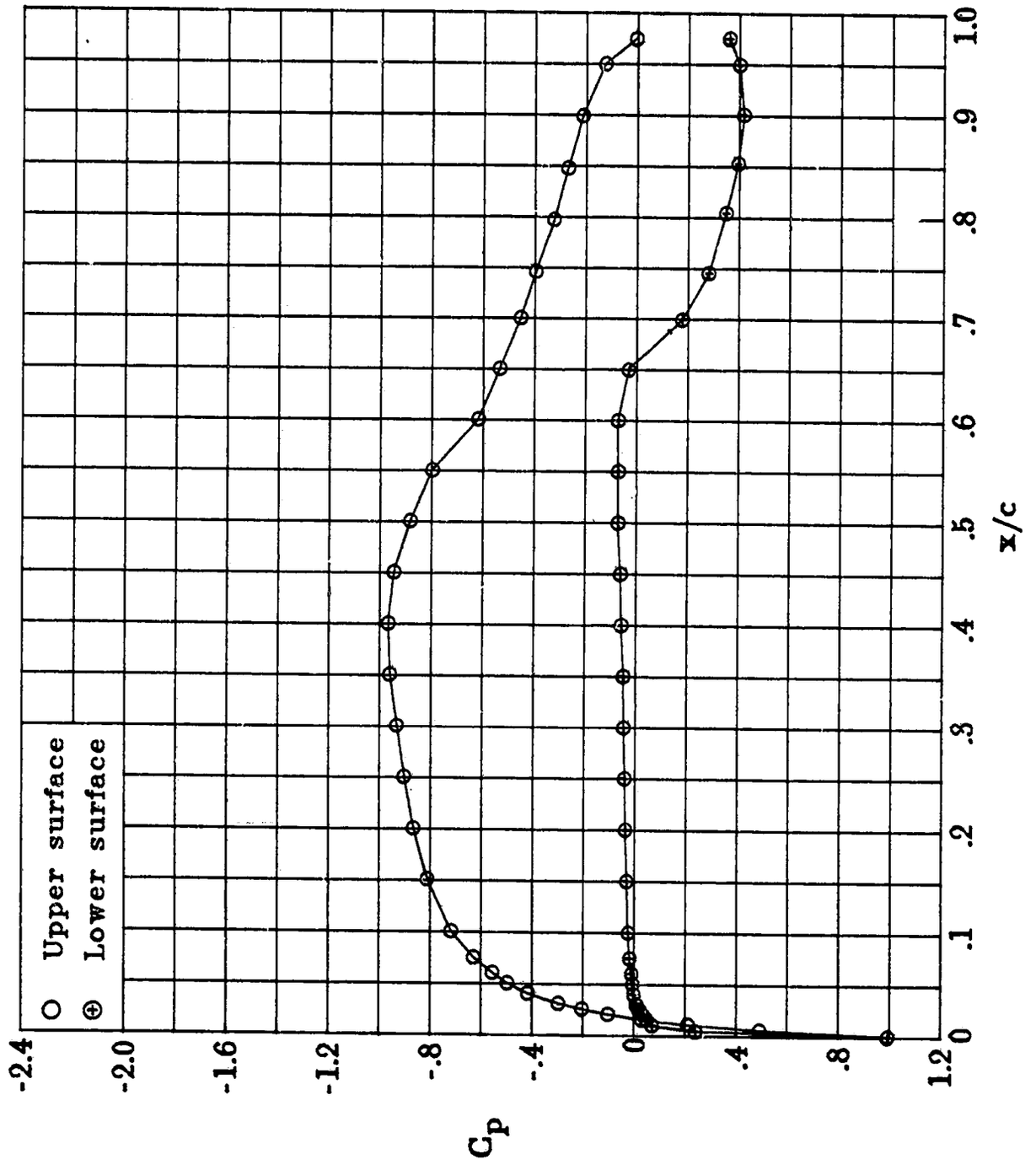

Figure 4.- Pressure distribution for NLF(1)-0215F airfoil at $\alpha = 0.0°$ for $R = 3.0 \times 10^6$ and $M = 0.10$.

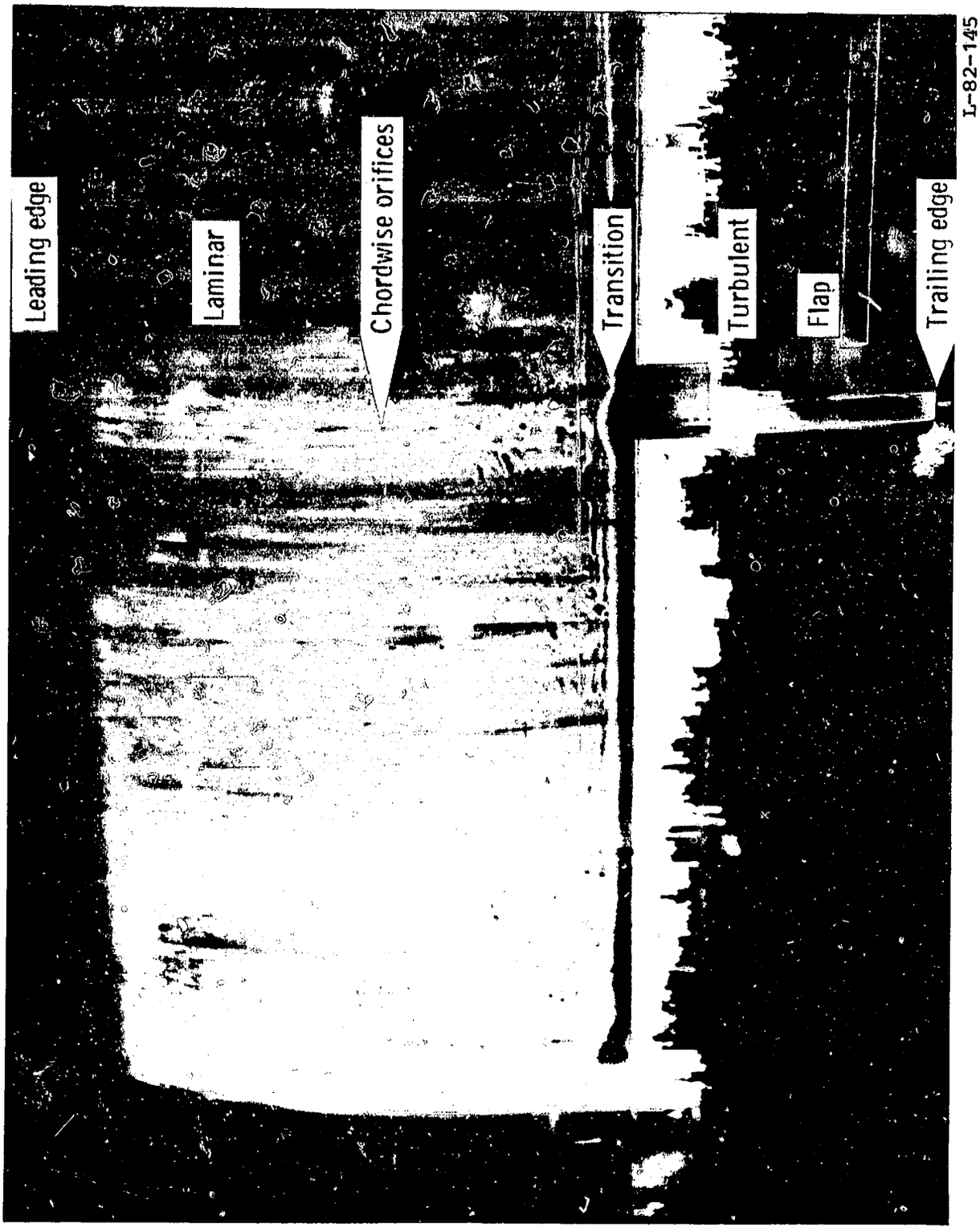

(a) $R = 0.5 \times 10^6$; $M = 0.04$.

Figure 5.- Oil-flow photographs of upper surface of NLF(1)-0215F airfoil at $\alpha = 0.0°$.

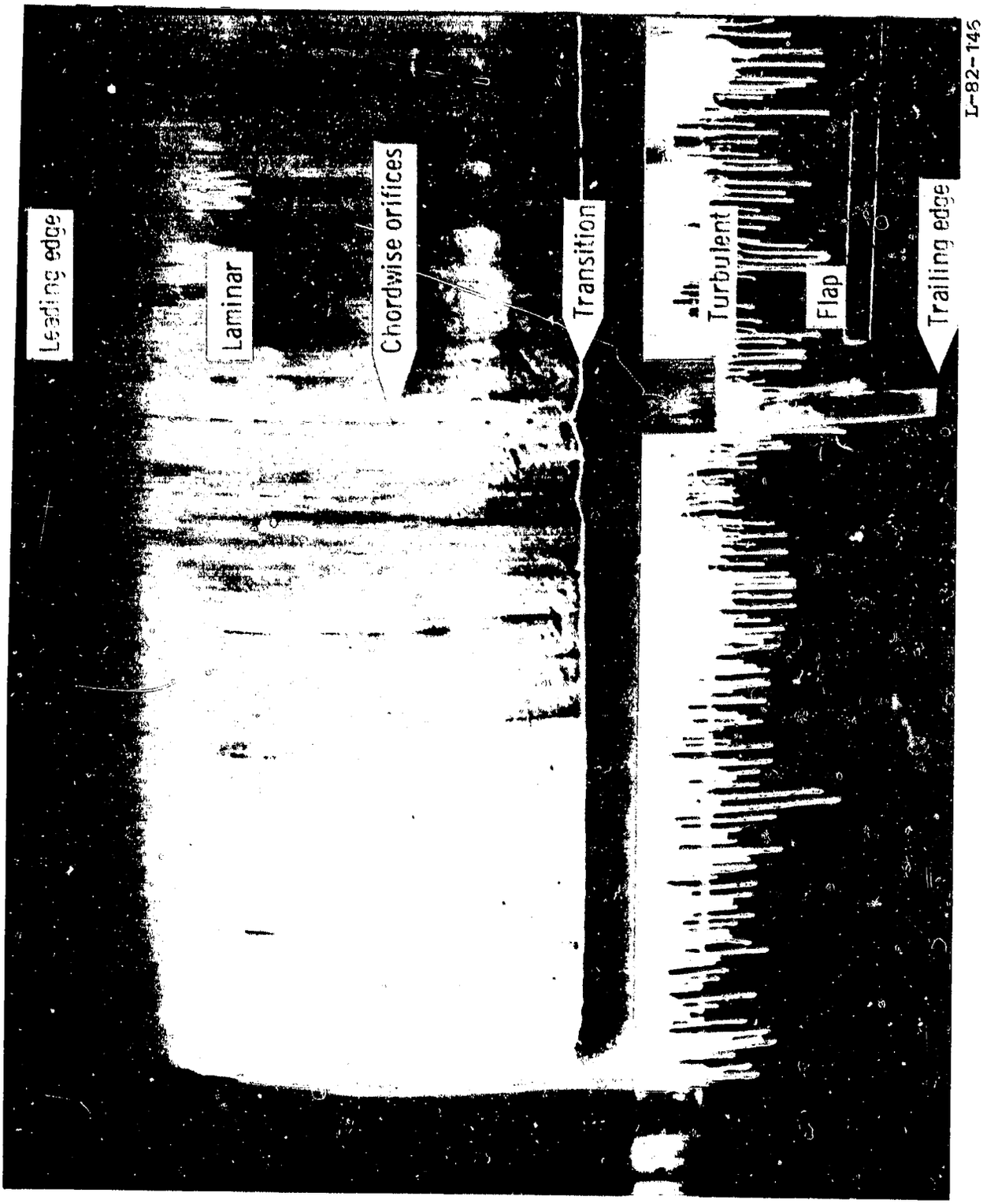

(b) $R = 1.0 \times 10^6$; $M = 0.07$.

Figure 5.- Continued.

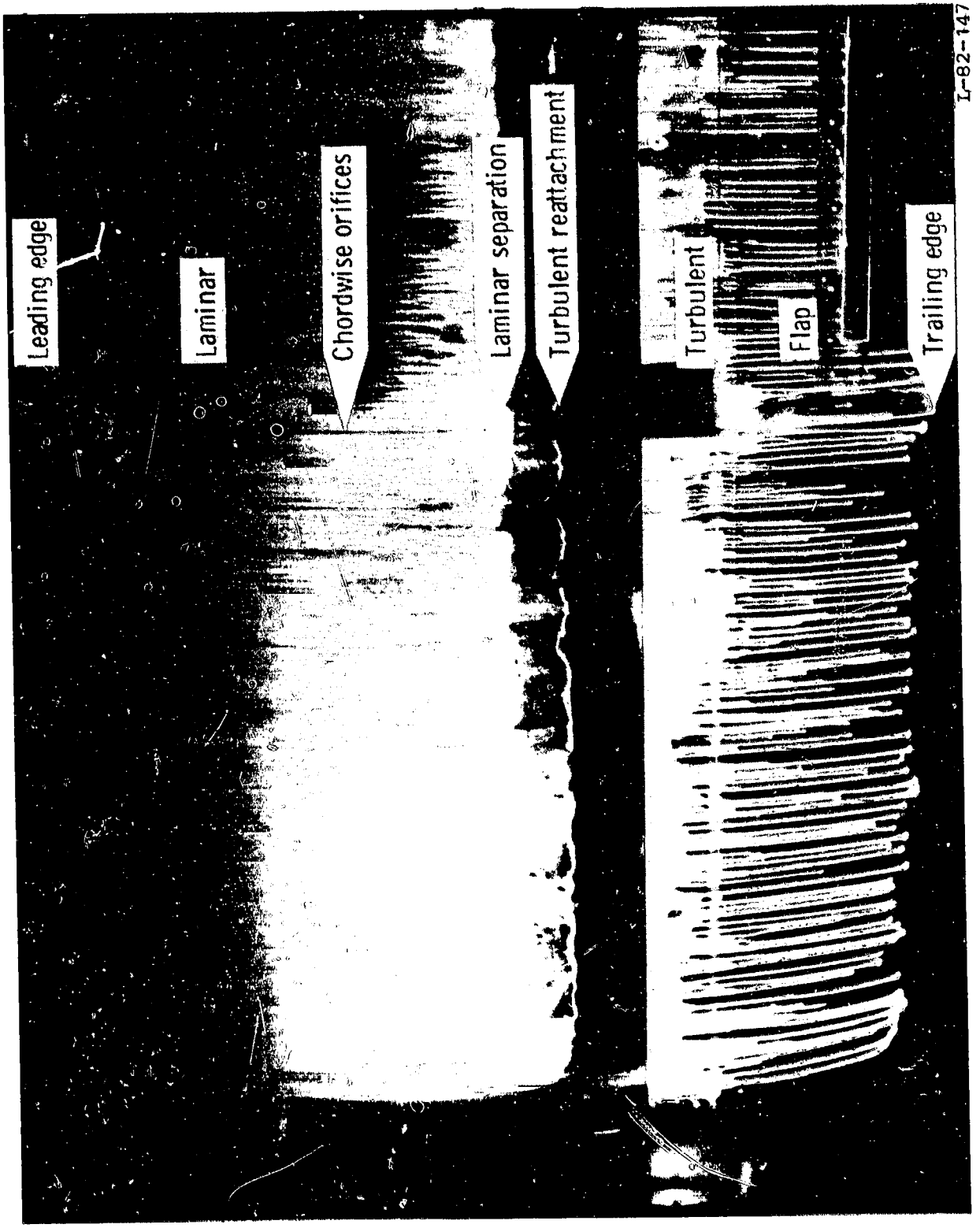

(c) $R = 1.5 \times 10^6$; $M = 0.10$.

Figure 5.- Continued.

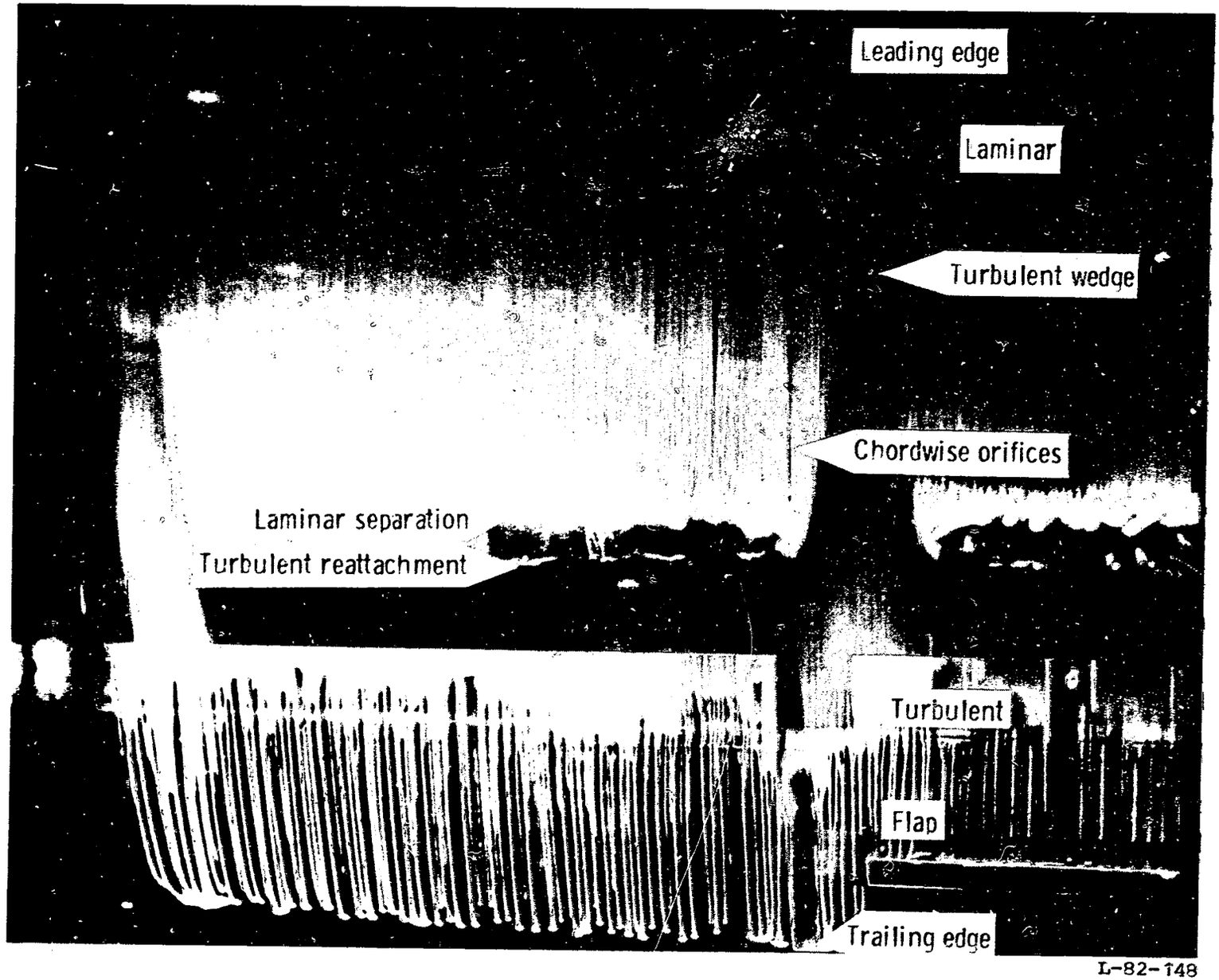

L-82-148

(d) $R = 2.0 \times 10^6$; $M = 0.14$.

Figure 5.- Continued.

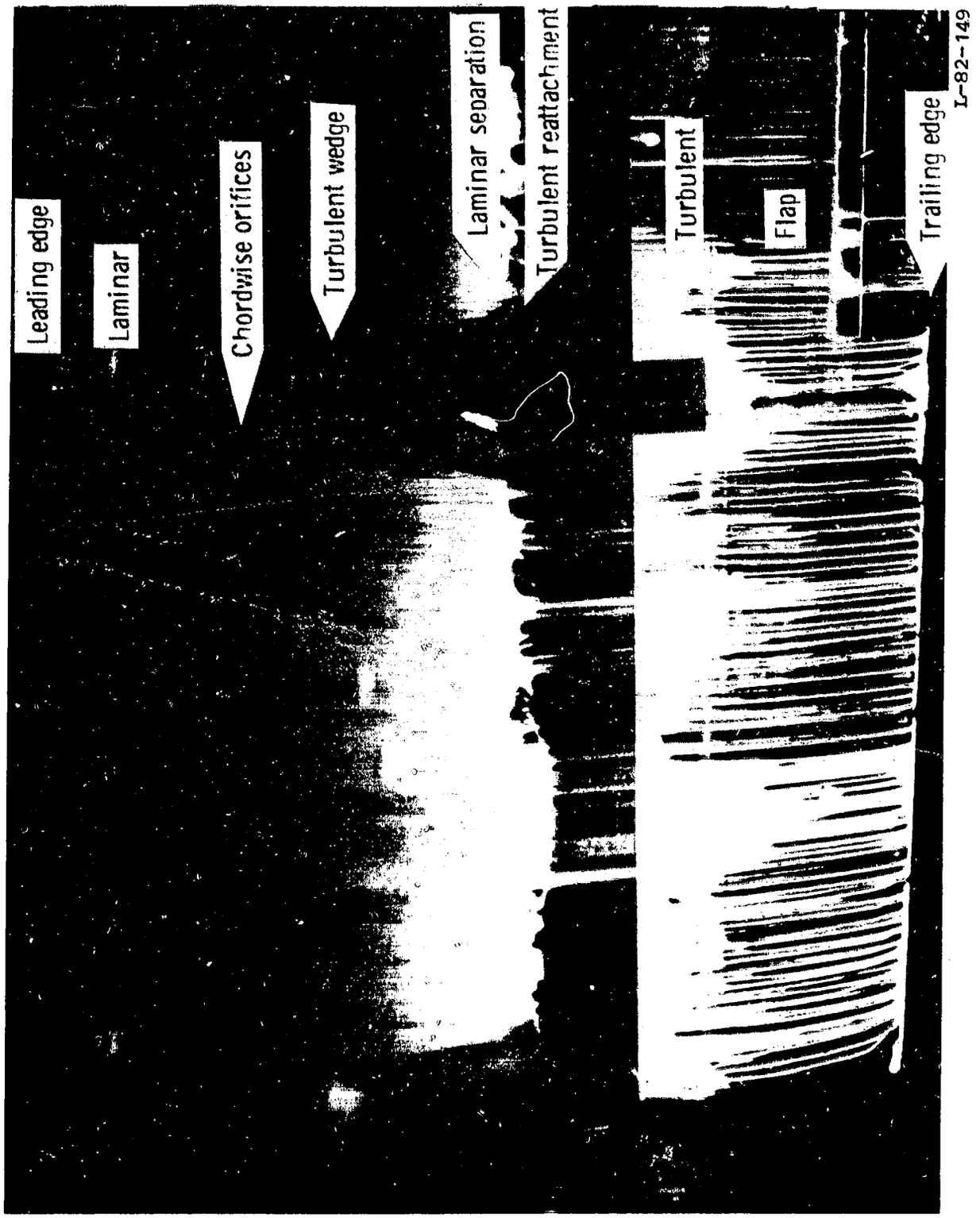

(e) $R = 3.0 \times 10^6$; $M = 0.21$.

Figure 5.- Continued.

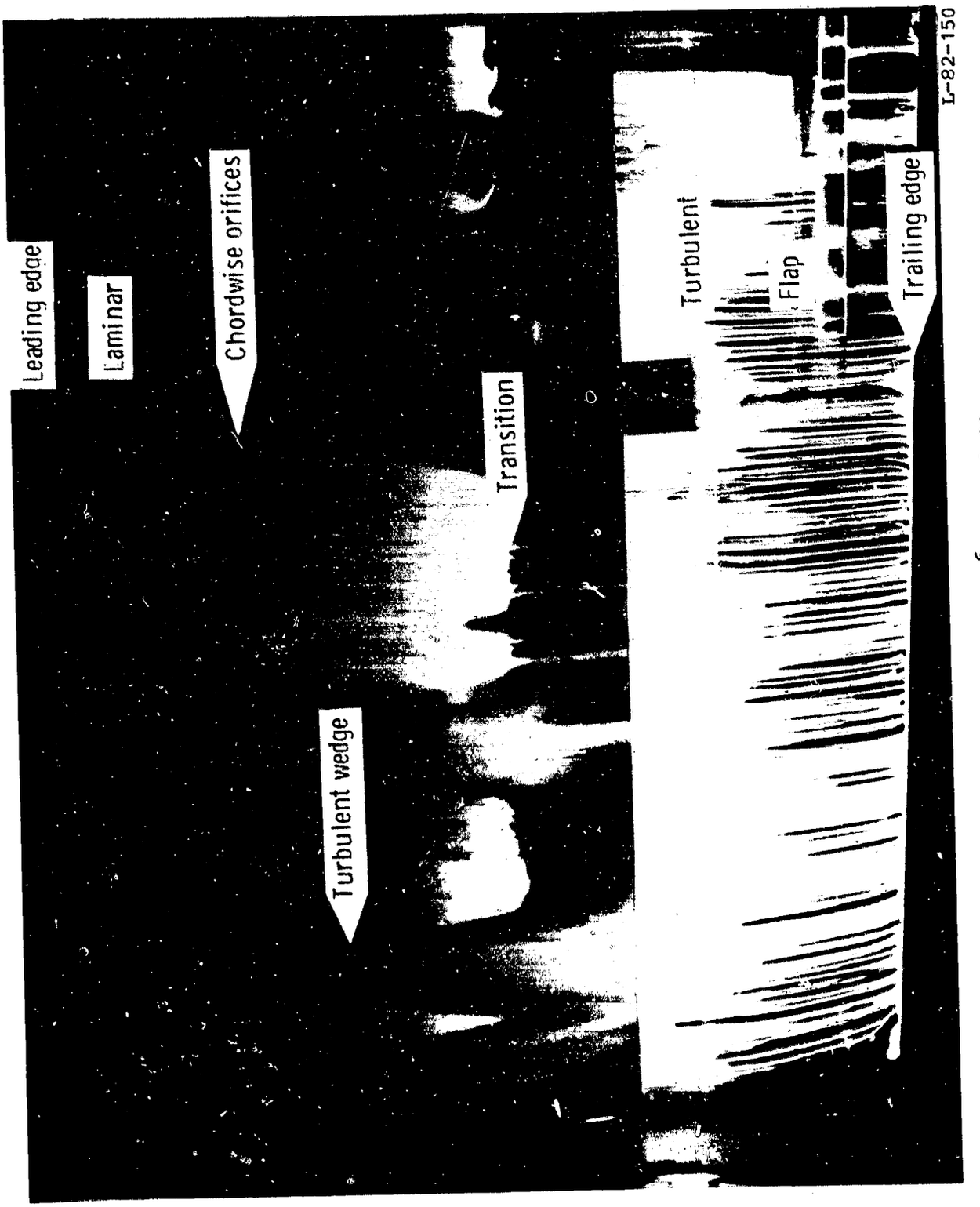

(f) $R = 4.0 \times 10^6$; $M = 0.28$.

Figure 5.- Concluded.

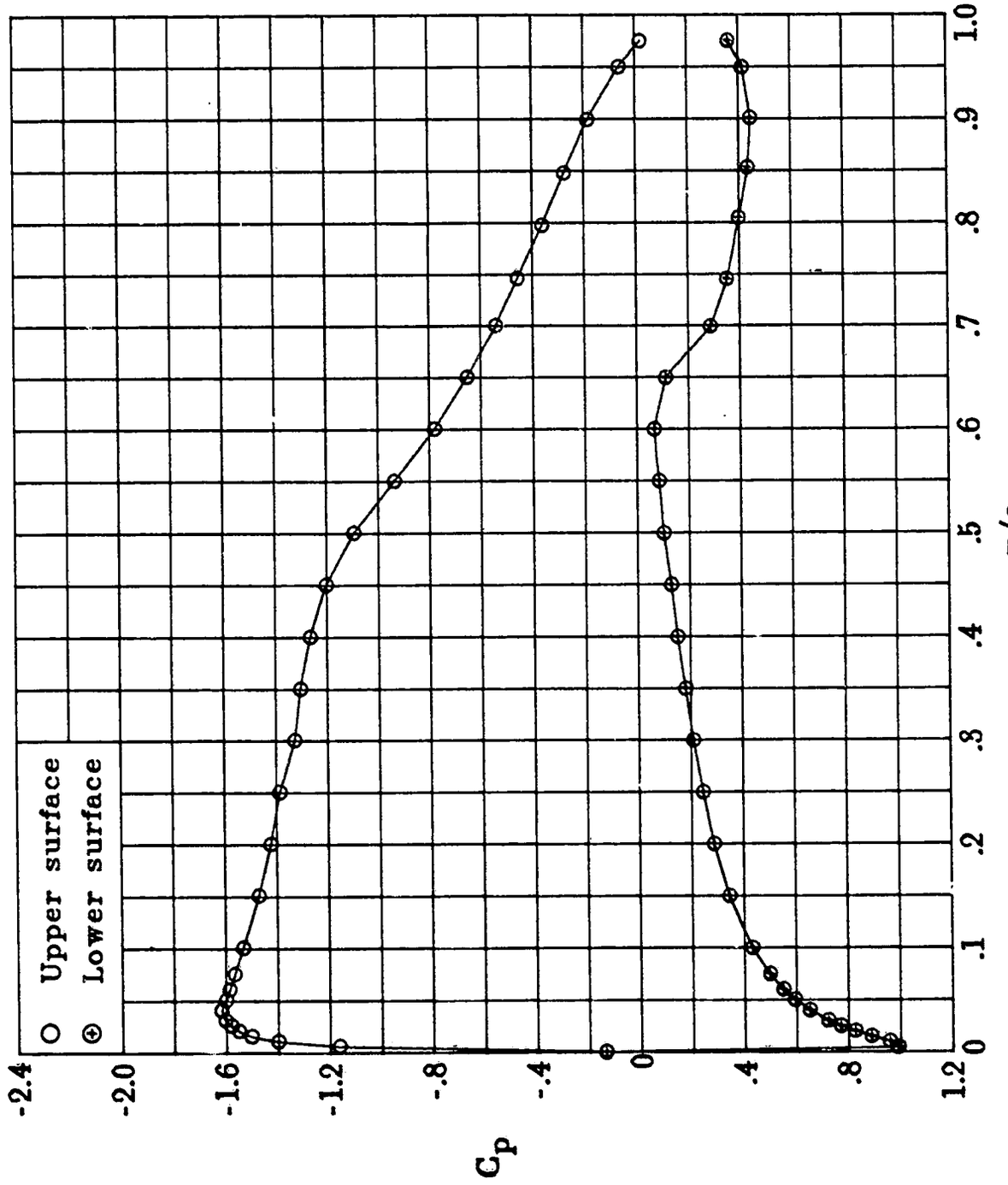

Figure 6.- Pressure distribution for NLF(1)-0215F airfoil at $\alpha = 5.0°$ for $R = 3.0 \times 10^6$ and $M = 0.10$.

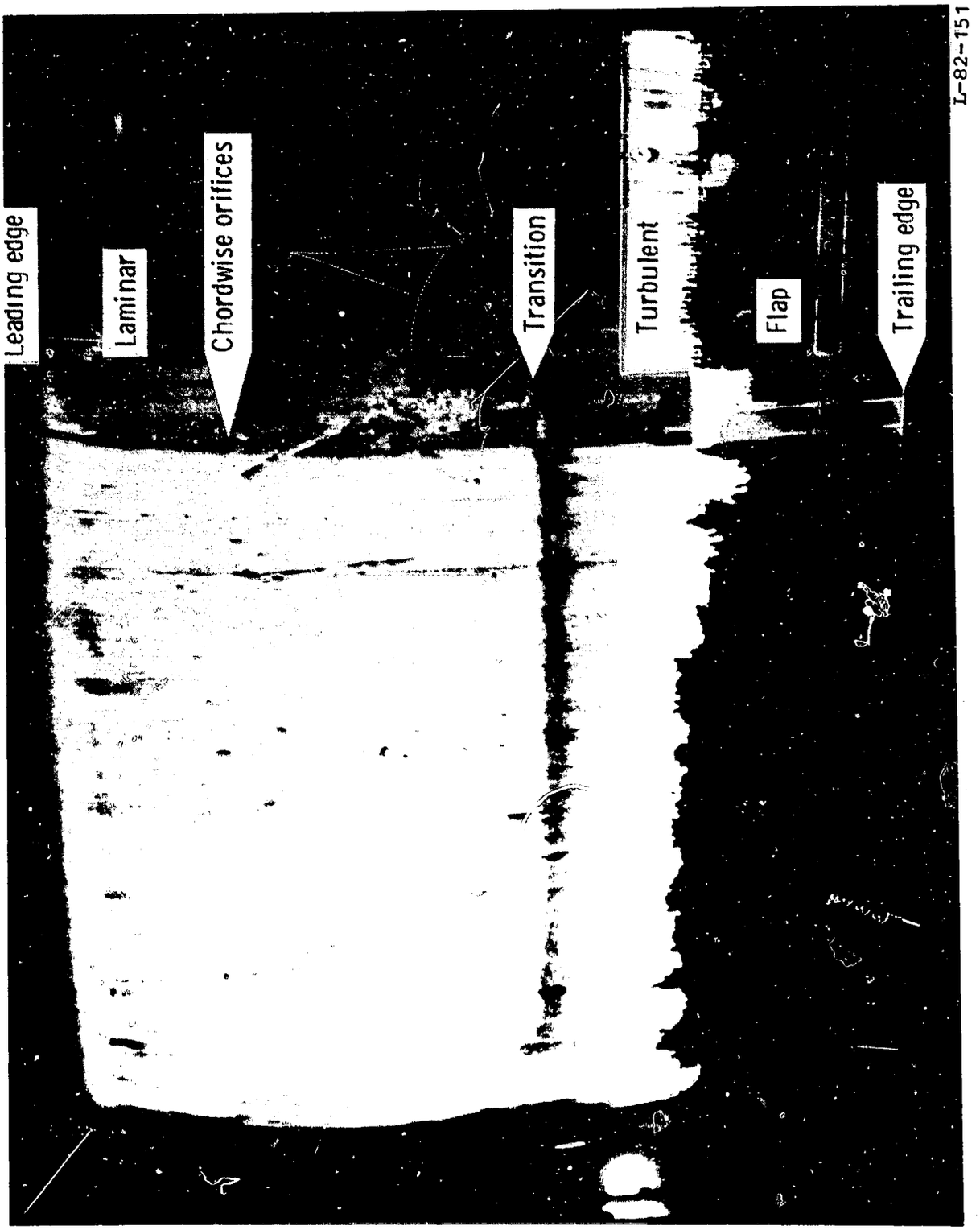

(a) $R = 0.5 \times 10^6$; $M = 0.03$.

Figure 7.- Oil-flow photographs of upper surface of NLF(1)-0215F airfoil at $\alpha = 5.0°$.

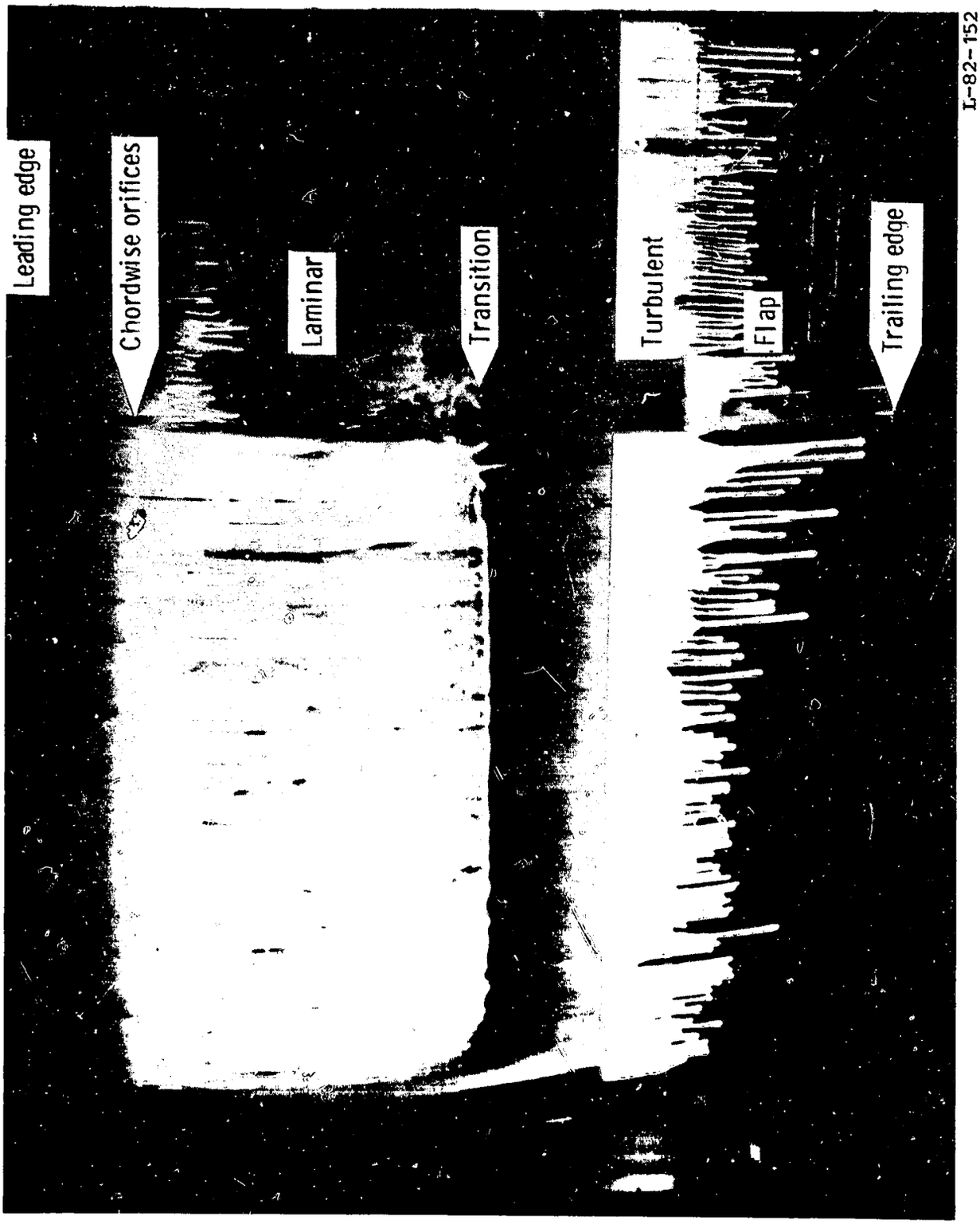

(b) $R = 1.0 \times 10^6$; $M = 0.07$.

Figure 7.- Continued.

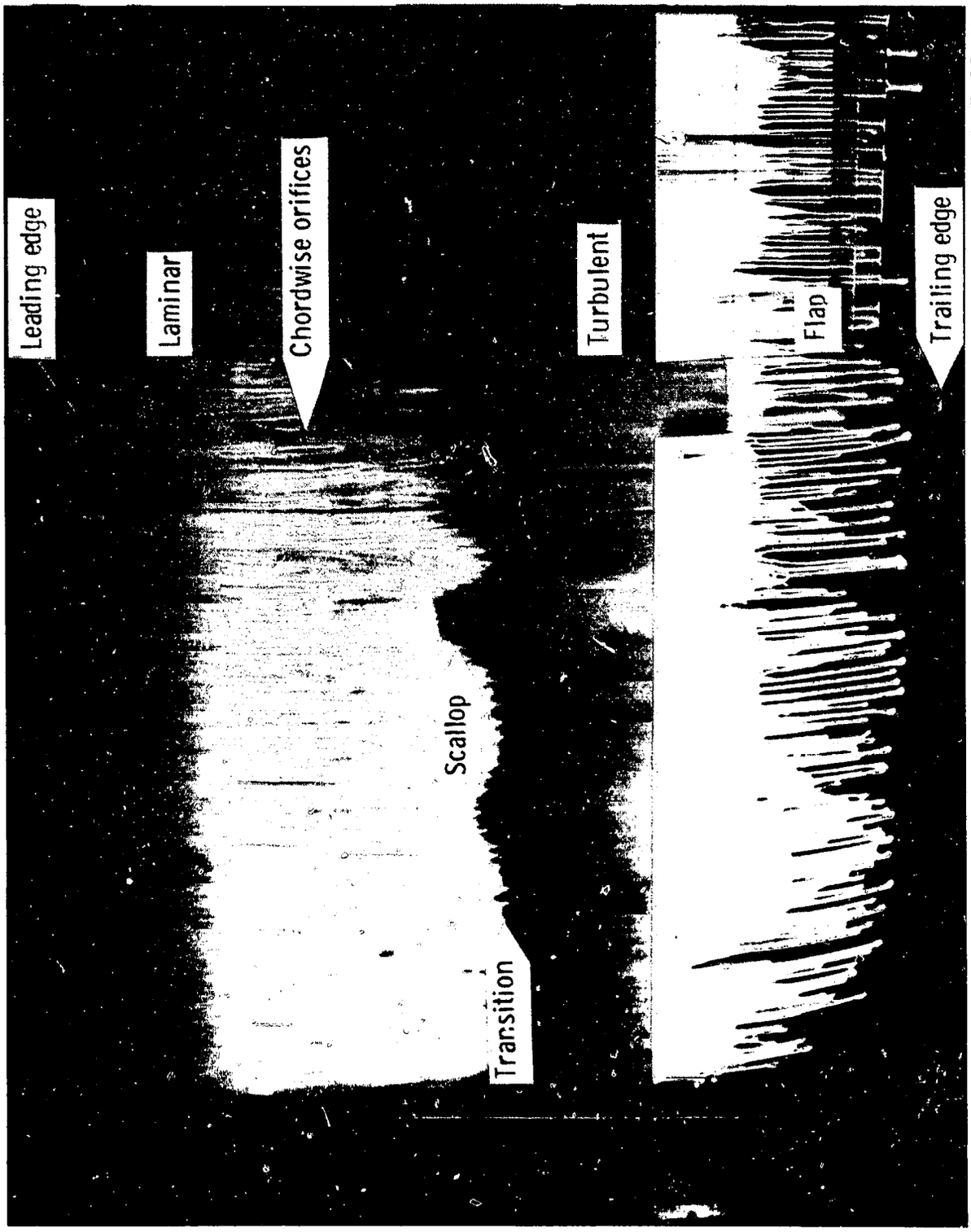

(c) $R = 1.5 \times 10^6$; $M = 0.10$.

Figure 7.- Continued.

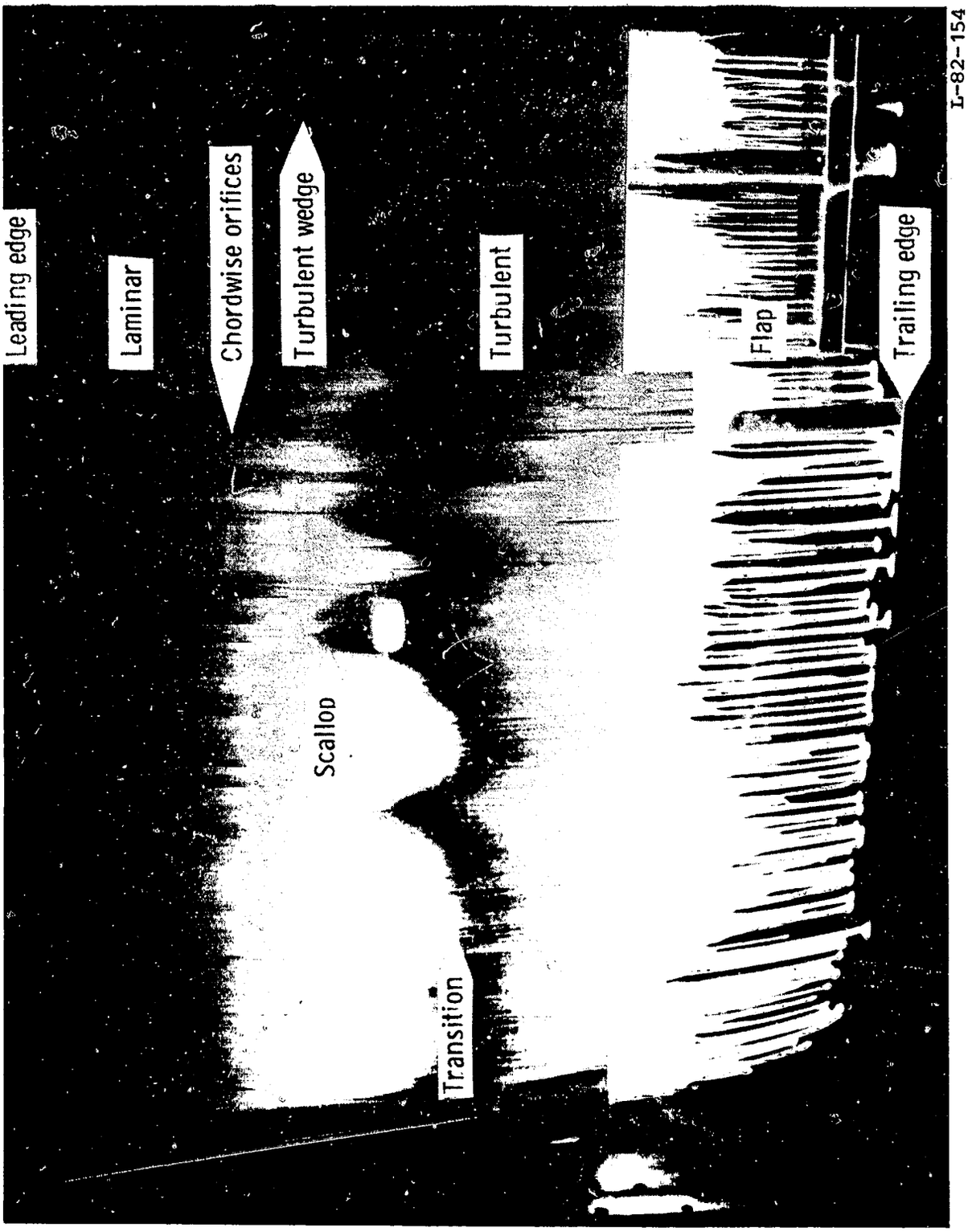

(d) $R = 2.0 \times 10^6$; $M = 0.14$.

Figure 7.- Continued.

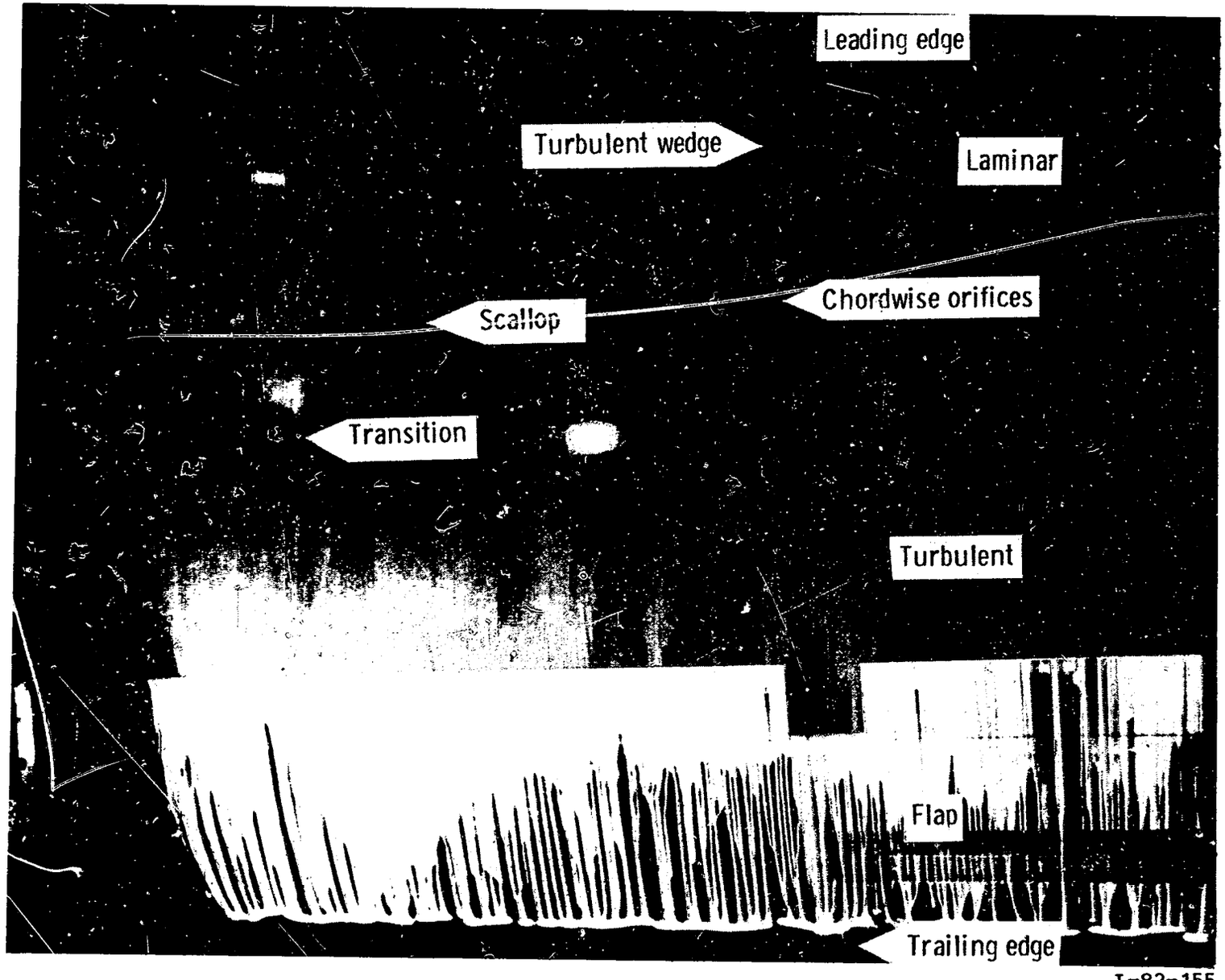

L-82-155

(e) $R = 3.0 \times 10^6$; $M = 0.20$.

Figure 7.- Continued.

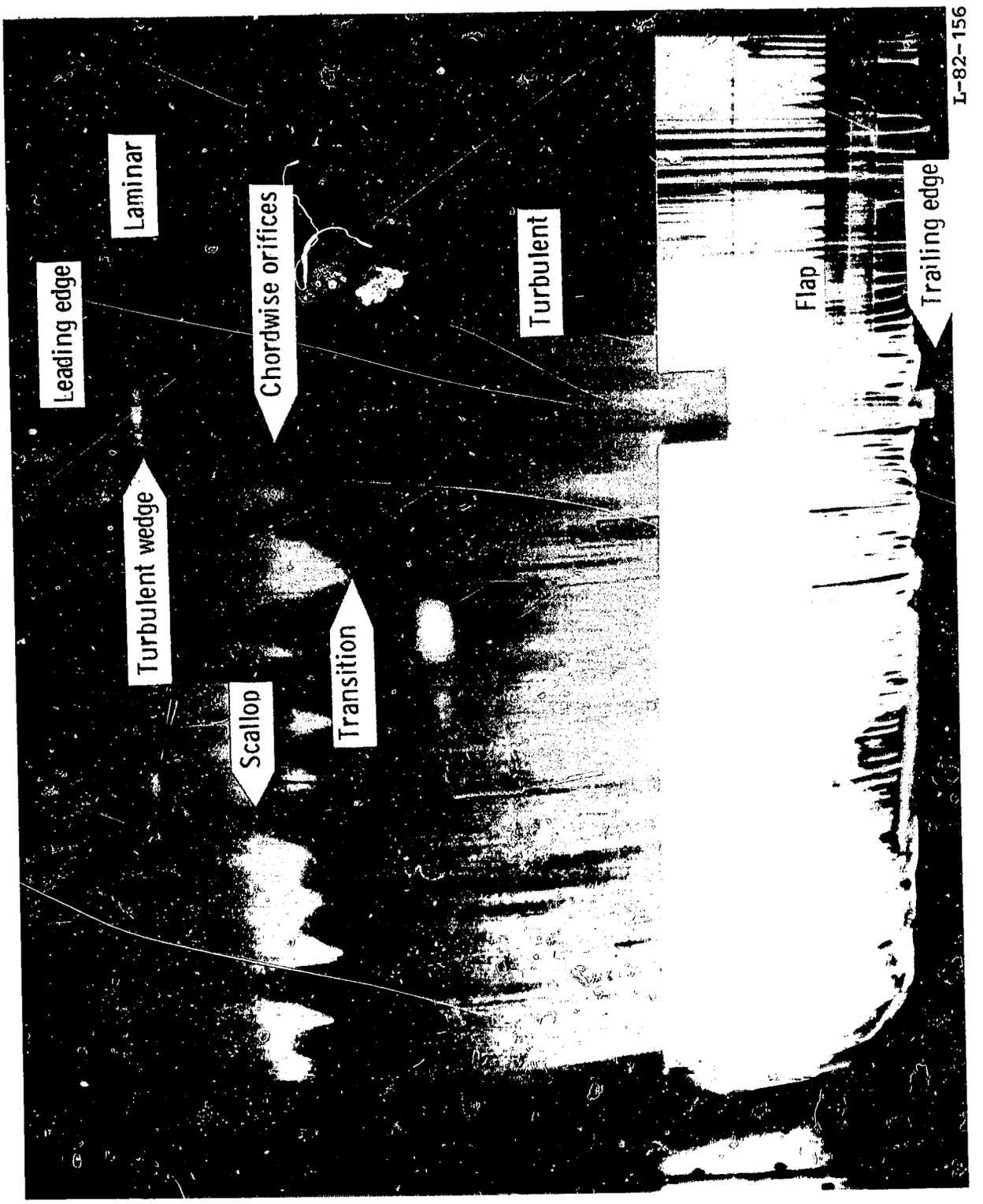

(f) $R = 4.0 \times 10^6$; $M = 0.28$.

Figure 7.- Continued.

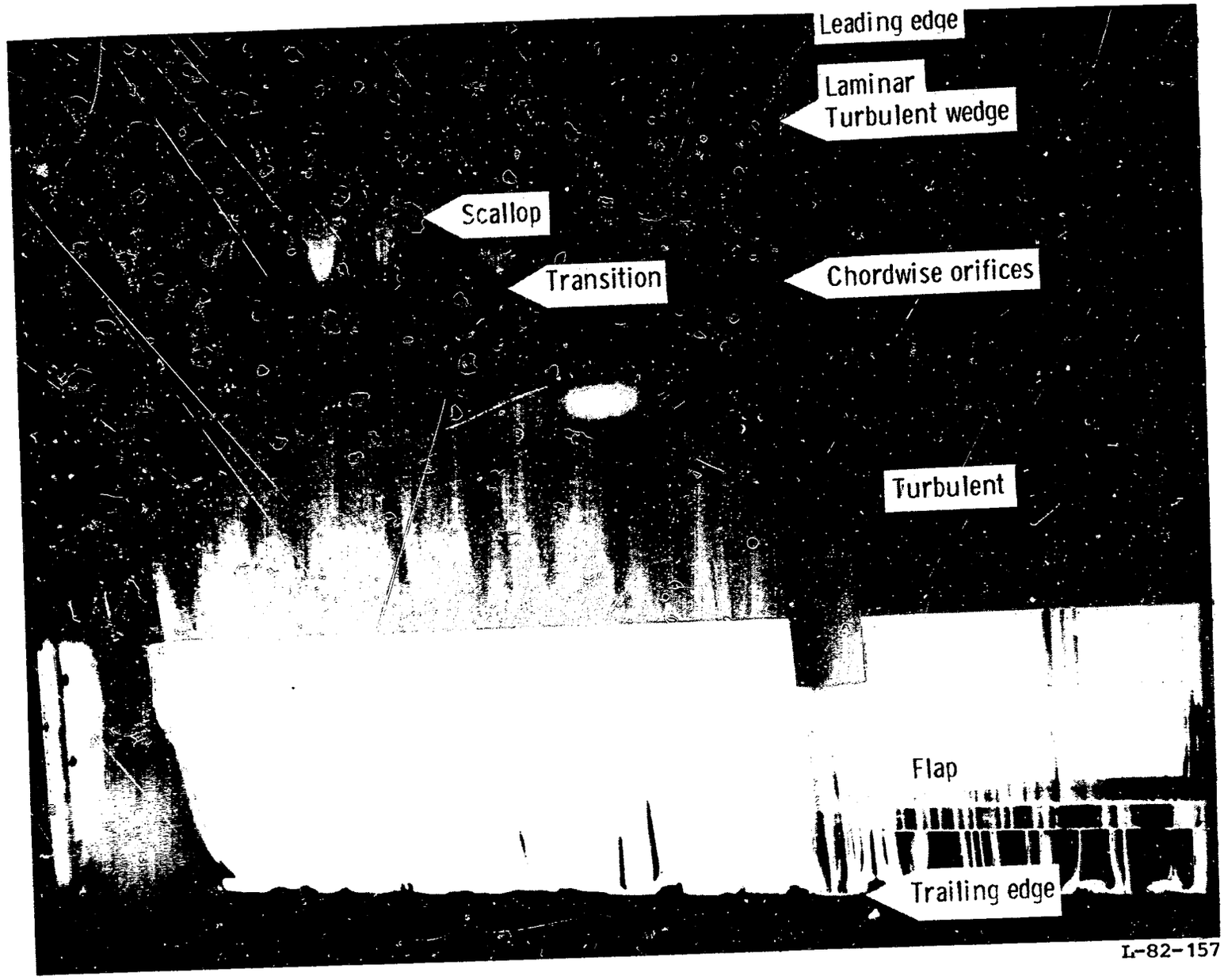

(g) $R = 6.0 \times 10^6$; $M = 0.42$.

Figure 7.- Concluded.

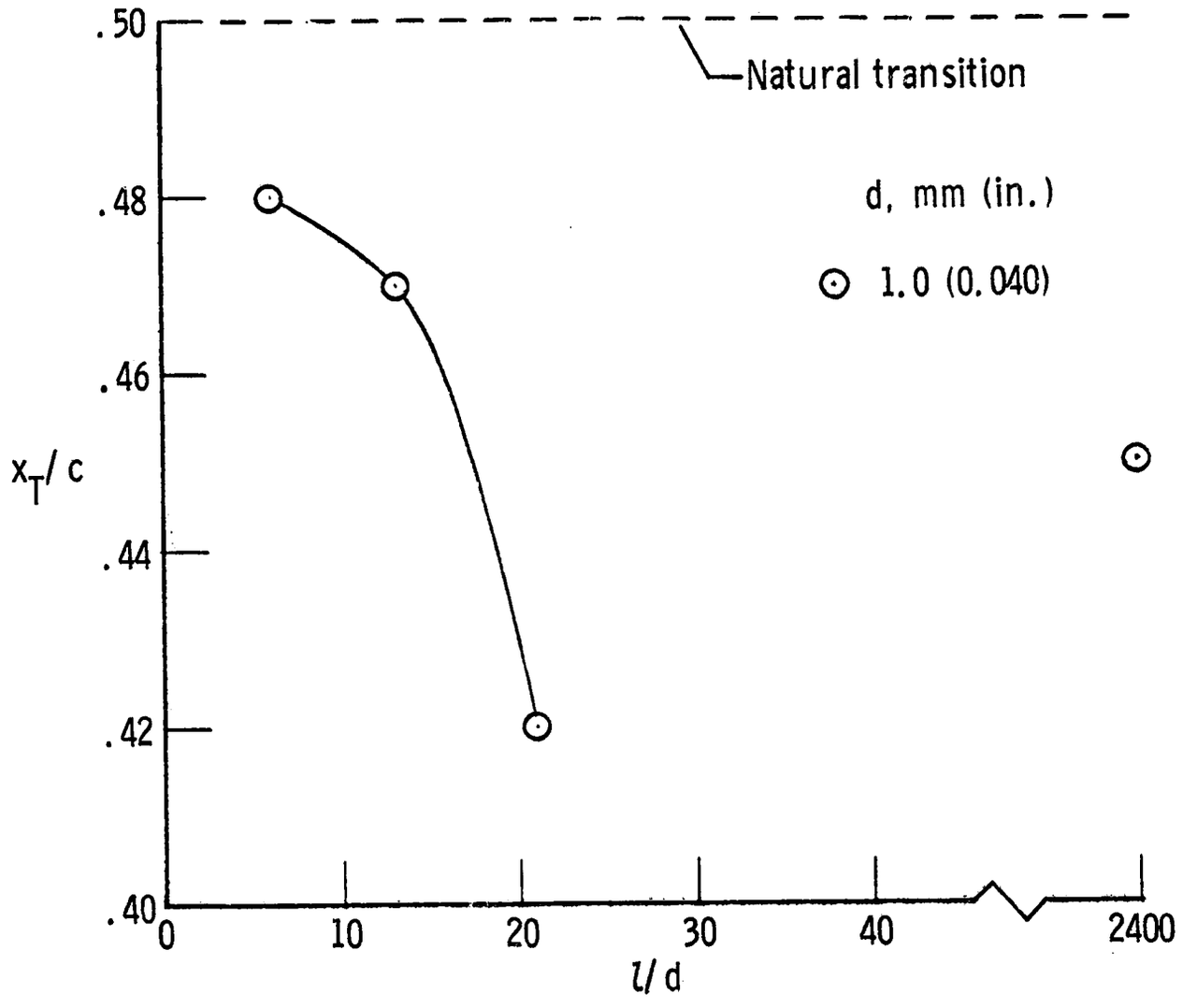

(a) $R = 1.5 \times 10^6$; $M = 0.10$.

Figure 8.- Effect of length-to-diameter ratio for single orifice on transition location on upper surface of NLF(1)-0215F airfoil at $\alpha = 5°$.

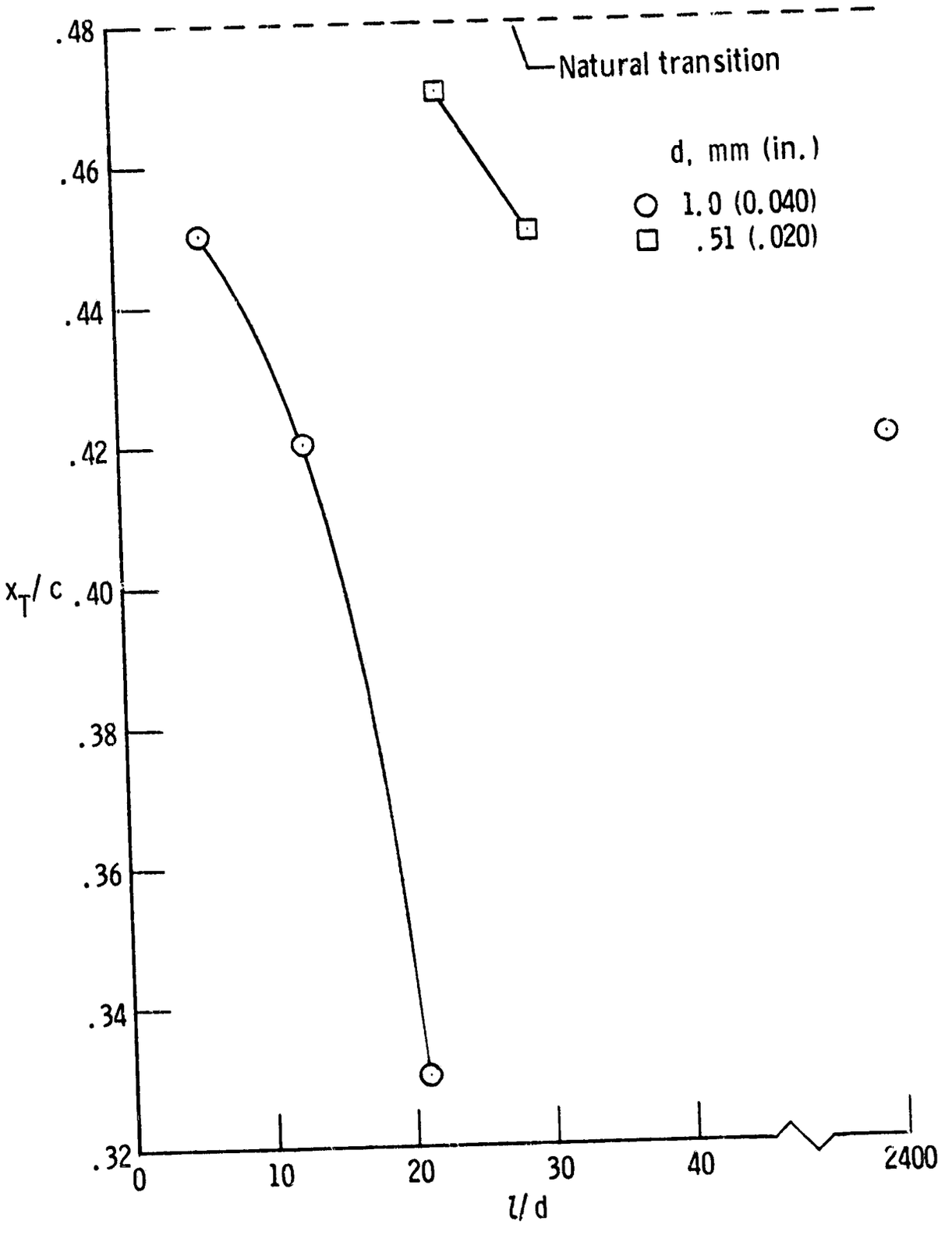

(b) $R = 2.0 \times 10^6$; $M = 0.14$.

Figure 8.- Continued.

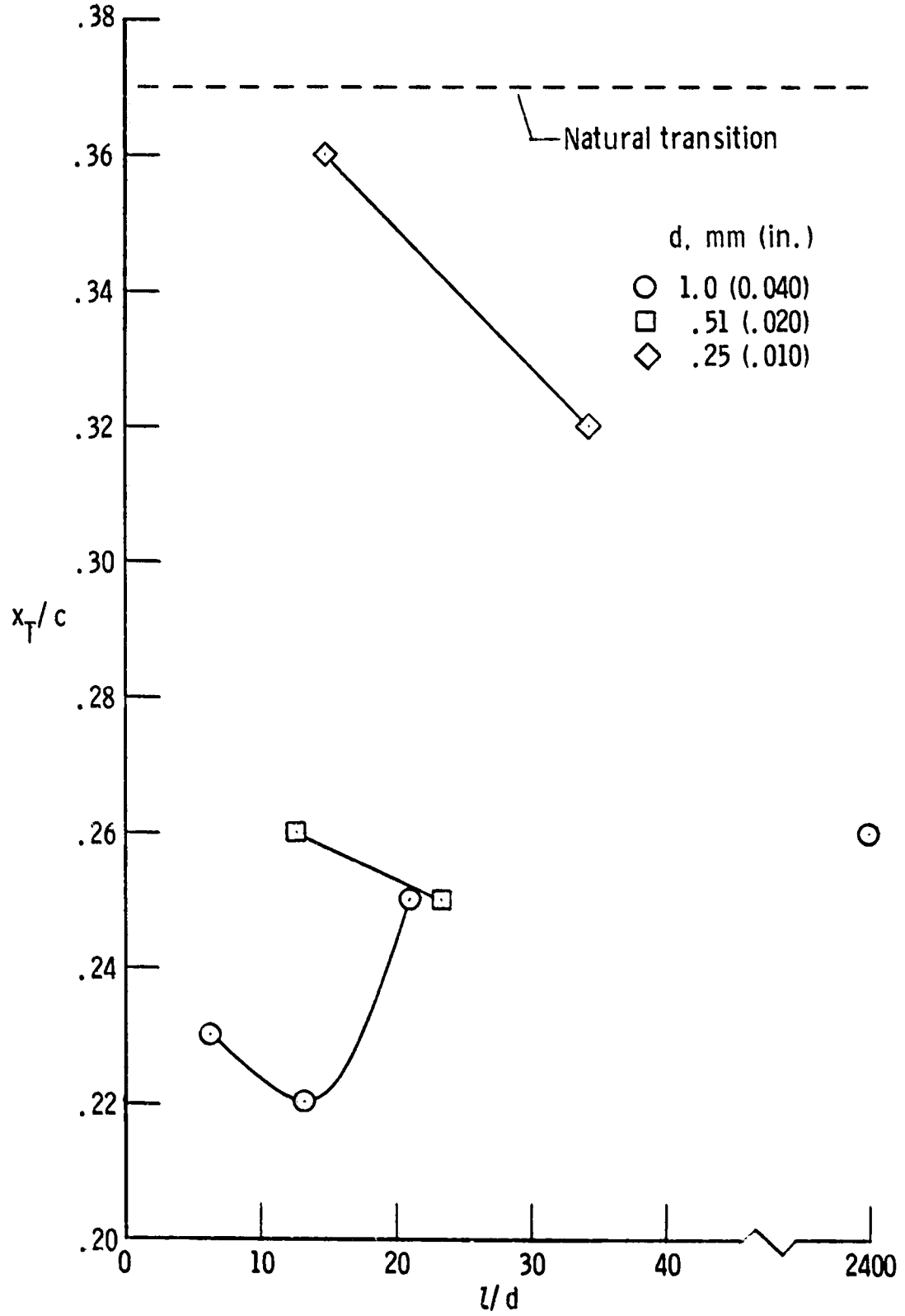

(c) $R = 3.0 \times 10^6$; $M = 0.20$.

Figure 8.- Continued.

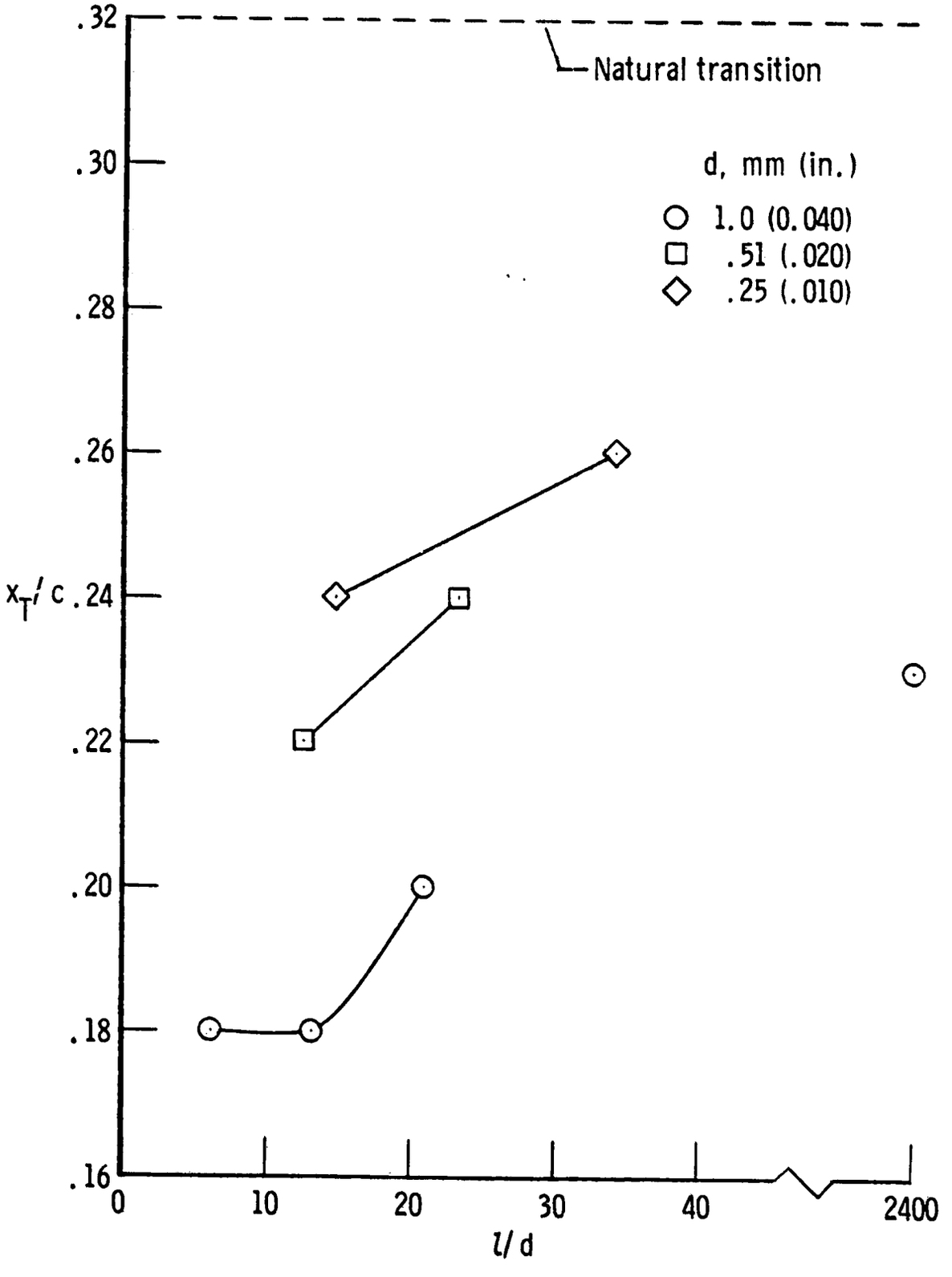

(d) $R = 4.0 \times 10^6$; $M = 0.28$.

Figure 8.- Continued.

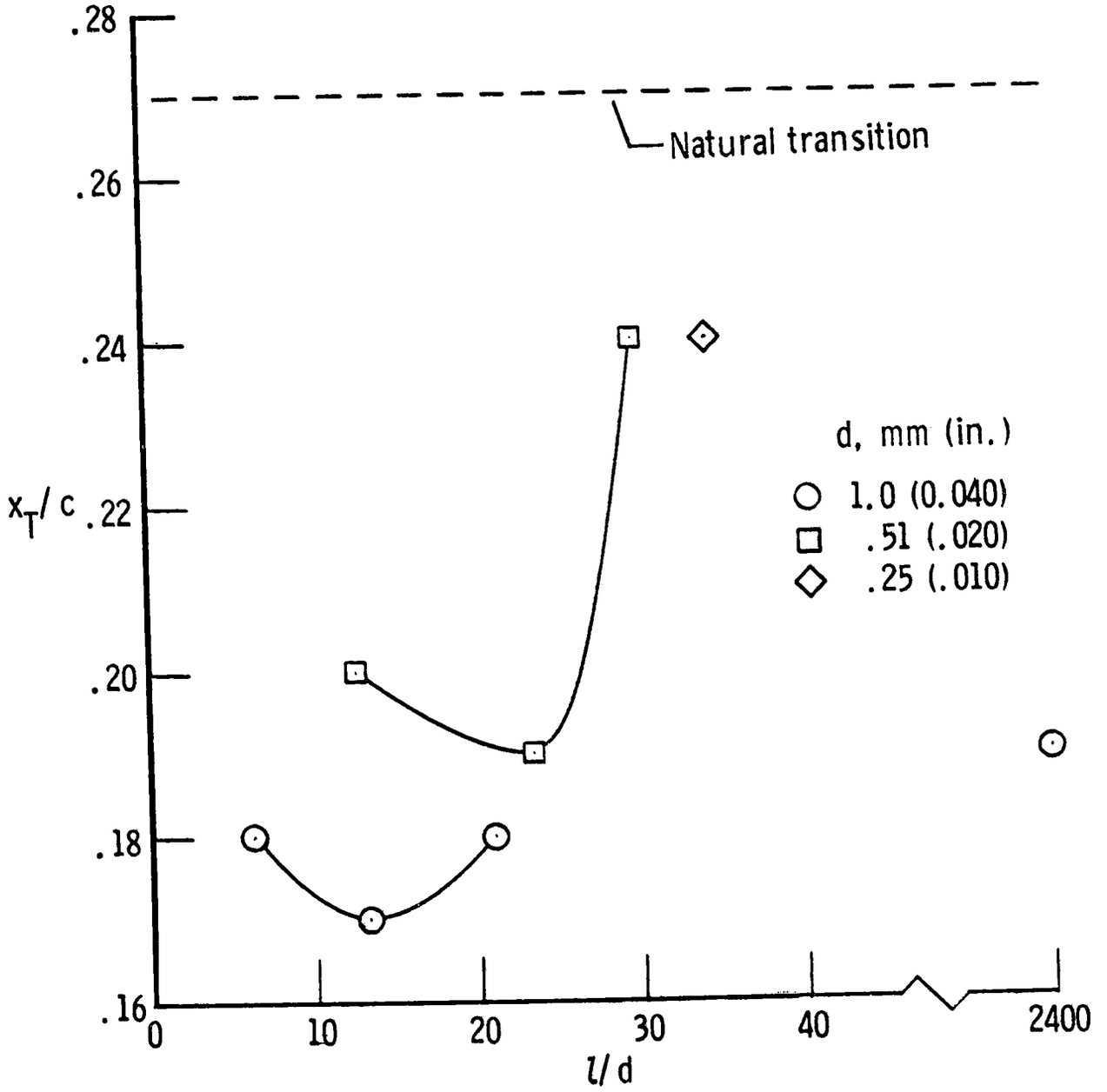

(e) $R = 6.0 \times 10^6$; $M = 0.42$.

Figure 8.- Concluded.